Nuclear Instruments and Methods in Physics Research B 121 (1997) 349–356

NIM B
Beam Interactions with Materials & Atoms

New large area ultraviolet lamp sources and their applications

Ian W. Boyd, J.Y. Zhang

Electronic and Electrical Engineering, University College London, Torrington Place, London WC1E 7JE, UK

Abstract

Dielectric barrier discharges are used to generate ultraviolet radiation in rare gases and rare gas-halide mixtures. The characteristics of the emission spectra of the excimers formed, from 126 to above 308 nm are found to be useful for thin film and surface processing. The underlying radiation generation mechanisms are described and the influence of gas mixture, concentration and total pressure on the UV emitted discussed. Conversion efficiencies (from input electrical to output optical energy) as high as 15% can be achieved under optimum conditions. These low cost, high power excimer systems can provide an interesting and potentially very useful alternative to conventional UV lamps for industrial large-scale low temperature processes.

1. Introduction

Photon-induced processing has become an accepted technology in a wide range of industrial sectors including automobile manufacturing, textiles, water and food treatment, electronics, chemicals, and medical treatment. Much of this processing has been performed with narrow wavelength CO_2, Nd:YAG, Ar ion, or excimer laser radiation [1–7]. Such lasers, however, are generally very expensive and provide only small area beams (typically only several cm^2). On the other hand, more broad-band radiation is available from high-current arc discharges in xenon and mercury/rare-gas mixtures which emit radiation ranging from 200 nm to several microns. However, since many materials absorb radiation at wavelengths shorter than about 250 nm, very efficient UV or deep UV sources are very desirable for stimulating chemical processes. Therefore, there is a demand for high-power, efficient, low cost and large-area UV and VUV sources.

Very recently, a new generation of lamps has been developed [8–15], based on the excited dimer (excimer) mechanism. These are capable of producing high power, high efficiency, and narrow-band radiation from the near UV ($\lambda \approx 354$ nm) to the deep UV ($\lambda = 126$ nm). It is well known that excimers, which are unstable excited molecular complexes, can be generated in a number of ways, e.g., by dielectric barrier discharges (also known as silent discharges), high energy electron beams, X-rays, synchrotron radiation, protons, heavy ions, α-particles and microwave discharges [16–22]. Of these, the silent discharge method has enormous potential for industrial applications because of its simplicity, high efficiency and low cost. Kogelschatz and Eliasson [8,9,13–15,23,24] have investigated many different excited species including rare-gas dimers (e.g. Ar_2^*, Kr_2^*, and Xe_2^*), halogen dimers (e.g. F_2^*, Cl_2^*, Br_2^*, and I_2^*), and rare-gas halide excimers (e.g. ArF^*, $ArCl^*$, $KrCl^*$, $XeCl^*$, etc.) as well as mercury halogen excimers ($HgNe^*$, $HgAr^*$, $HgKr^*$, and $HgXe^*$) using dielectric barrier discharges. The underlying principles of these sources will be described here, and examples of their possible applications will be given.

2. The excimer system

The operating principle followed in our work relies on the radiative decomposition of excimer states created by a silent discharge in a high pressure (few hundred mbar) gas column [24]. In a dielectric barrier discharge lamp, one or both electrodes must be electrically insulated, e.g. covered by a dielectric. A high voltage (7 to 10 kV) and high frequency (100 to 500 kHz) supply is then applied to the device causing an arc discharge to occur. The charge build-up on the dielectric surface immediately decreases the field in the discharge gap and extinguishes the arc. The total duration of a typical arc is of the order of a few nanoseconds and several arcs can be formed quasi-simultaneously yet randomly across the entire surface of the dielectric at a frequency equal to two times the driving frequency. Each individual current filament is described as a microdischarge because of the short time duration and low electrical energy it involves. The self-extinguishing feature of this type of discharge enables the use of high (≈ 500 mbar) gas pressure without causing any sputtering of the electrodes and therefore erosion and contamination problems common with traditional arcs are eliminated.

Many styles and shapes of excimer lamps can be fabricated. In many of our experiments, these are cylindrical, and the UV generated radiates outwards. A typical lamp is composed of two concentric quartz tubes, outer

0168-583X/97/$17.00
PII S0168-583X(96)00538-1

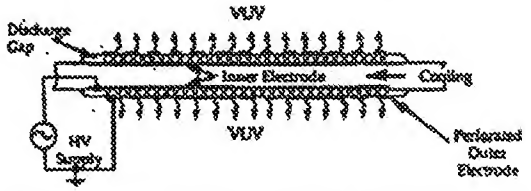

Fig. 1. General geometry of a cylindrical excimer lamp source.

and inner metallic electrodes, an external high voltage generator, and cooling water (Fig. 1). The measured energy conversion efficiencies (UV output/electrical input) for these lamps can be as high as 15%. In the case of rare gas halide mixtures circulating between the electrodes, and in particular for the mixtures of ArF, KrF and XeCl, the well-known excimer laser frequencies of 192, 248 or 308 nm are obtained. For excited molecular complexes in pure rare gases, lower wavelength continua are generated at 126, 146 and 172 nm for argon, krypton and xenon respectively. The bandwidth associated with these emissions is typically around 10–20 nm.

The pumping mechanism involved in the formation of rare gas excimers in the case of xenon, used in our current studies, is illustrated by Fig. 2 [25], while Fig. 3 shows a simplified potential energy diagram for this system. Note the absence of any bound ground level for the Xe_2 dimer, which indicates splitting when emission occurs. Therefore self-absorption of the radiation by the gas phase is completely absent in this system [26].

The schematic of Fig. 2 summarises the following operations (1)–(6). Energetic electrons present in the microdischarges excite and ionise the xenon atoms:

$$e^- + Xe \rightarrow Xe^* + 2e^-, \quad (1)$$

$$e^- + Xe \rightarrow Xe^+ + e^-. \quad (2)$$

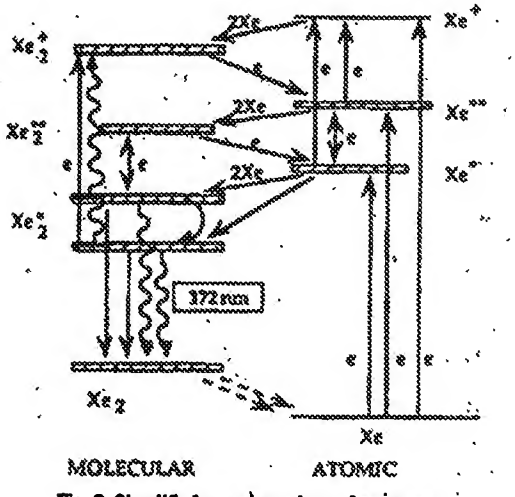

Fig. 2. Simplified pumping scheme for xenon.

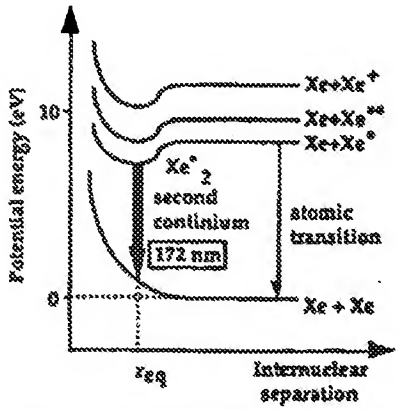

Fig. 3. Simplified band diagram of xenon.

At pressures above 30 mbar (relevant to our case) the formation of molecular ions is rapid and subsequently leads to the formation of excited neutrals:

$$Xe^+ + 2Xe \rightarrow Xe_2^+ + Xe, \quad (3)$$

$$Xe_2^+ + e^- \rightarrow Xe^{**} + Xe. \quad (4)$$

The creation of the rare gas dimer, Xe_2^*, then occurs through the three body reaction of an electronically excited rare gas atom Xe^* with two others in the ground state:

$$Xe^* + Xe + Xe \rightarrow Xe_2^* + Xe. \quad (5)$$

The Xe_2^* excimer consequently dissociates into Xe atoms and radiates a 172 nm photon:

$$Xe_2^* \rightarrow 2Xe + h\nu \quad (172\ nm). \quad (6)$$

A potential energy diagram for rare-gas/halogen excimers is shown in Fig. 4. The $X_{1/2}$ ground state arises from the ground state ^1S of the rare-gas and the ^2P level ($s = 1/2$, $l = 1$, $m_l = 0$) of the halogen atom. The $A\ ^2P_{1/2,3/2}$ state comes from ^1S rare-gas and ^2P ($s = 1/2$, $l = 1$, $m_l = \pm 1$) halogen atom. The three close lying excited states ($B_{1/2}$, $C_{3/2}$, and $D_{1/2}$) are generated by a positive rare gas ion ^2P and a negative halogen ion $^1S\ X^-$ (X = F, Cl, Br, I). The transitions from $B_{1/2}$, $C_{3/2}$, and $D_{1/2}$ to $A_{1/2,3/2}$ and $X_{1/2}$ and their associated wavelengths are shown in Table 1 [25,27].

The intensity and spectral half-width values of the radiation generated from various transitions is very different. For example, the $D_{1/2} \rightarrow X_{1/2}$ transition generates the shortest wavelength while its intensity is much less than that of the $B_{1/2} \rightarrow X_{1/2}$ transition, indicating that the upper level is quenched by collisions to lower states in the ionic manifold. The $B_{1/2} \rightarrow X_{1/2}$ transition is the strongest because the initial and final $p\sigma$ orbitals which the electron occupies have the largest overlap of any of the valence orbitals [25]. Weaker broadband emissions via $C_{3/2} \rightarrow A_{3/2}$ and $B_{1/2} \rightarrow A_{1/2}$ transitions are also present. These overlap strongly for fluoride and chloride excimers but are

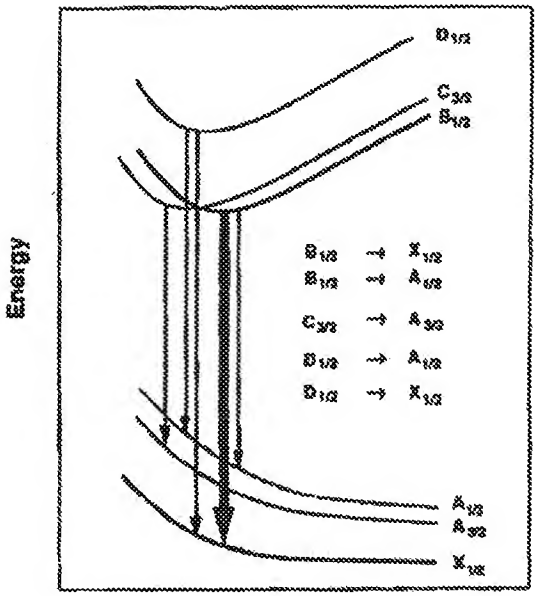

Fig. 4. Simplified potential energy scheme of rare-gas halides and corresponding excimer transitions (the widths of the lines indicate relative intensities).

quite separate for bromide and iodide systems. Radiation can also generated by formation of Rg_2X^* species, such as triatomic Kr_2Cl^*. As shown by the spread in Table 1, such emission is much more broadband.

The reaction mechanisms underlying the formation of excited rare-gas halides are complex, involving several ground state atomic and molecular species, several ionic species, and large numbers of excited atomic and molecular species. Firstly, as shown in (7)–(9) below, where Rg represents a rare-gas species (e.g. Ar, Kr, Xe) and X a halogen (e.g. F, Cl, Br, and I), the high energy electrons ionize and excite the rare-gas and halogen species.

$$e^- + Rg \rightarrow Rg^* + e^-, \quad (7)$$

$$e^- + Rg \rightarrow Rg^+ + 2e^-, \quad (8)$$

$$e^- + X_2 \rightarrow X + X^-. \quad (9)$$

Most RgX^* exciplexes (excited complexes) can be created by a three-body recombination of the positive rare-gas ions and the negative halogen ions (10) or the harpooning reaction (11) in which the excited rare-gas species transfers its loosely bound electron to the halogen molecule or halogen-containing compound to form an electronically excited state of RgX^* [25], as shown:

$$Rg^+ + X^- + M \rightarrow RgX^* + M, \quad (10)$$

$$Rg^* + X_2 \rightarrow RgX^* + X, \quad (11)$$

where M is a collisional third partner which in many cases can be an atom or molecule of the active species or even of the buffer gas. The excimer or exciplex molecules formed are not very stable and rapidly decompose, typically within a few nanoseconds, giving up their excitation energy in the form of a UV photon, i.e.

$$RgX^* \rightarrow Rg + X + h\nu(UV). \quad (12)$$

The radiation process competes with several quenching processes. At low pressures, the dominant quenching mechanism is direct quenching by the halogen-bearing species. Thus,

$$RgX^* + X_2 \rightarrow Rg + 3X. \quad (13)$$

However, at high pressures three-body reactions involving the rare-gas atoms quench the excited rare-gas halides by forming triatomic species.

$$RgX^* + 2Rg \rightarrow Rg_2X^* + Rg. \quad (14)$$

Table 1
Main peak wavelengths of rare-gas (Rg) halide excimers at high pressures [25,27]

Rg	X	RgX^*				Rg_2X^* (nm)
		$D_{1/2} \rightarrow X_{1/2}$ (nm)	$B_{1/2} \rightarrow X_{1/2}$ (nm)	$C_{3/2} \rightarrow A_{3/2}$ (nm)	$B_{1/2} \rightarrow A_{1/2}$ (nm)	
Ne	F	106	108	110	111	~ 145
Ar	F	185	193	203	204	290 ± 25
Ar	Cl		175		195	245 ± 15
Ar	Br		165	172	183	
Kr	F	220	248	275	272	400 ± 35
Kr	Cl	200	222	240	235	325 ± 15
Kr	Br		207	222	228	~ 318
Kr	I		190	195	225	
Xe	F	264	351	460	418	610 ± 65
Xe	Cl	236	308	345	340	450 ± 40
Xe	Br	221	282	300	325	440 ± 30
Xe	I	203	253	263	320	~ 375

Table 2
Spread of wavelengths available with excimer sources, compared with a selection of bond-strengths of common molecules

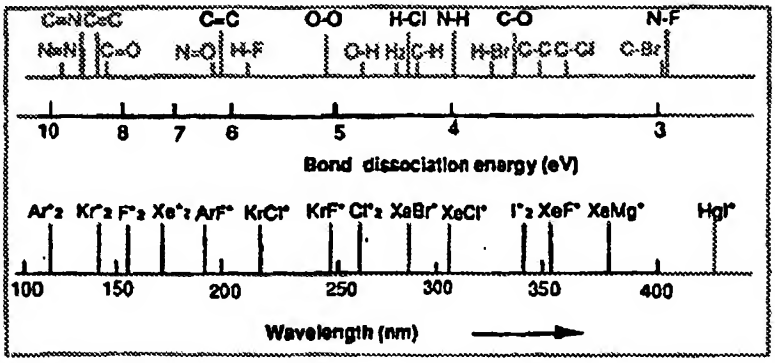

Table 2 summarizes the range of excimer wavelengths readily available with rare gas and rare gas-halides and compares these with the bond energies of various common molecules. Clearly, these sources can be utilised to directly excite and dissociate many types of materials.

3. Excimer lamp processing

The lamps system mainly used in this study contained Xe within the cylindrical geometry, as mentioned above. An inner dielectric-covered electrode was supplied by an external discharge voltage. The microdischarges induced upon breakdown created the 172 nm photons which were emitted through the outer dielectric, chosen to be Suprasil® quartz, known to be transparent to the radiation generated. The lamp output power, measured to be around 3 W (corresponding to 20 mW/cm^2), was determined using actinometric techniques. The generic experimental set-up used is sketched in Fig. 5.

The radiation generated was passed through a MgF_2 window into a reaction chamber where the host substrate, which could be heated to a temperature of 400°C, was placed. The cell could be evacuated to 10^{-6} mbar and filled with the appropriate gas mixtures for specific processing applications. For oxidation, pure oxygen is used, whilst for deposition, mixtures of of SiH_4, NH_3, O_2, and N_2O are employed. Ar was used as the purge gas. Thermocouple control ensured that, although essentially negligible, the low intensity of the lamp did not increase the

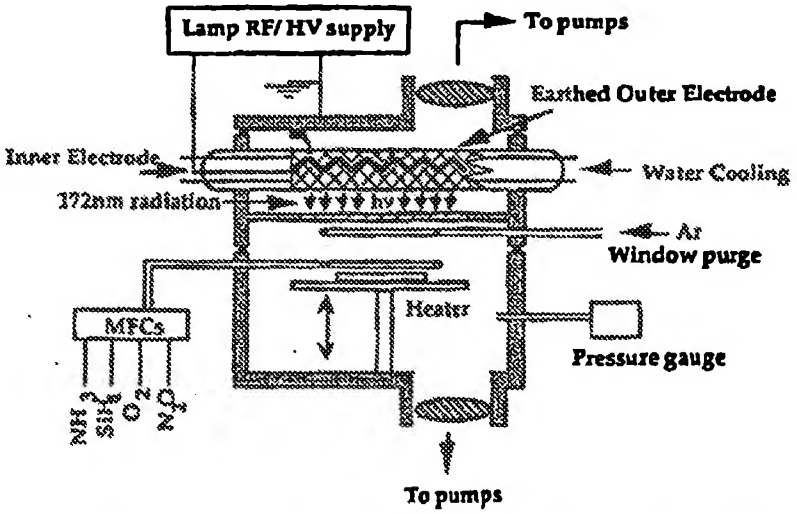

Fig. 5. General experimental arrangement used for photoprocessing of thin films and surfaces.

surface temperature of the samples during film growth. A full description of this reactor is published elsewhere [11].

4. Applications of excimer ultraviolet sources

4.1. UV-induced metal deposition

The prospect of depositing metal films and structures through photo-decomposition of spin-on metallo-organic or organometallic precursors has attracted much attention with respect to applications for high density multichip interconnects, printed circuit boards, high density packaging, multilayers, etc. Most of the work has been done using a laser either in air, oxygen, nitrogen, or other suitable atmospheres to convert the precursors into their constituent metal elements [28–30].

The fabrication of thin films by laser-induced metallo-organic decomposition (L-MOD) techniques offers several advantages over other thin film deposition processes. For example, it occurs at ambient temperature and pressure without the need for gas transport or distribution systems and therefore there is no need for complicated vacuum equipment. These precursor materials can be readily synthesised to incorporate a wide variety of metals. As already mentioned, however, lasers are very expensive, non-uniform sources and can only pattern limited areas. Therefore, the use of large-area UV sources with high photo fluxes for industrial large-area processing is very appealing.

Excimer UV lamp-induced decomposition of palladium acetate films has in fact recently been demonstrated [10,31–34]. The palladium thin films produced were a few nanometres thick and can act as the activator for subsequent electroless metal plating processing in which micrometer-thick copper, nickel or gold layer can be grown on top of the palladium. Such film thicknesses provide a level of electrical conductivity which is sufficient for applications such as microcircuits and printed circuit boards. It is well known that the activity of catalysts for electroless metal deposition depends on the thickness, distribution, and purity of the metal nuclei on the non-catalytical surface. The quality of the coating, e.g. the adhesion of the metal layers on the substrate depends decisively on the electrochemical properties of the Pd activator. Therefore, different excimer lamp parameters (wavelength, UV intensity, and exposure time) may have different effects on the thickness, morphology, and purity of the deposited palladium layers.

Fig. 6 shows the Pd thickness formed as a function of exposure time on quartz at different wavelengths ($\lambda = 172$ nm, $\lambda = 222$ nm, $\lambda = 308$ nm) [10,32–33,35]. The different deposition rates correlate with the different absorption coefficients at the wavelengths of the UV radiation, the highest being achieved for radiation at $\lambda = 172$ nm due to the higher absorption of palladium acetate in the vacuum ultraviolet. Structuring of these films can also be achieved

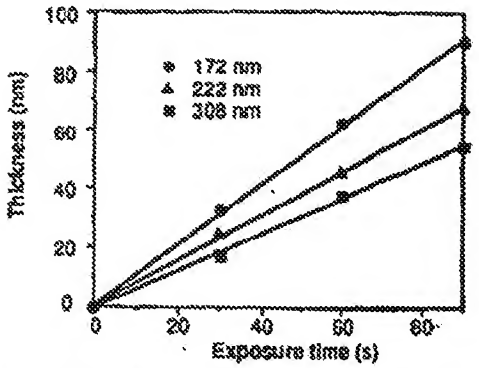

Fig. 6. Palladium thickness produced on quartz as a function of exposure time at different wavelengths; $\lambda = 172$ nm, $\lambda = 222$ nm, $\lambda = 308$ nm.

using metal contact masks. With this process, plastics, paper, polymer, cardboard or synthetic fibre can also be readily metal-coated at room temperature. Whilst the grain size of laser-irradiated Pd film is always large and the grains are arranged in clusters, by contrast, excimer UV sources always produce homogeneous and mirror-like films with a previously unattainable quality and adhesion [10,32]. The edge-definition of the Pd structures produced using excimer lamps is also highly reproducible and superior to that produced by excimer lasers [10,33].

4.2. Dielectric thin film deposition

Thin layers of silicon dioxide from silane and nitrous oxide mixtures or silane and oxygen mixtures [11,36] and of silicon nitride from silane and ammonia [37] have been successfully deposited using UV excimer lamps. The highest deposition rates (500 Å/min) have been achieved by irradiating silane and oxygen gas mixtures at a substrate temperature as low as 300°C [36]. Silane is in fact trans-

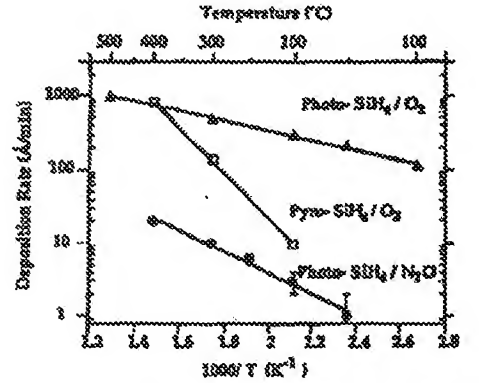

Fig. 7. Comparison of the deposition rate of SiO_2 for photo-CVD and thermal CVD.

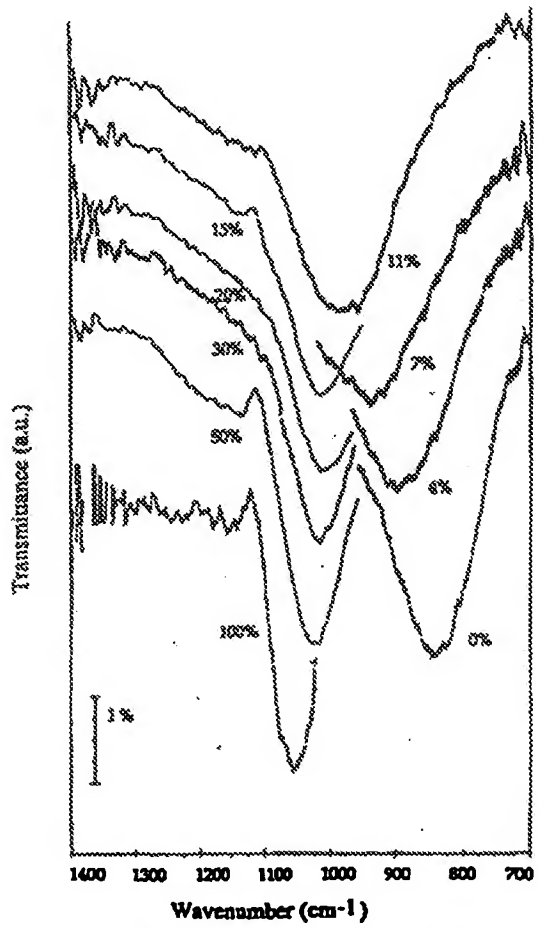

Fig. 8. Evolution of FTIR convoluted peak of Si–O stretch with Si–N stretch versus N_2O/NH_3 precursor ratio.

parent to 172 nm radiation, but the oxidising and reducing agents exhibit a significant absorption cross-section at this wavelength and are photochemically dissociated with this lamp.

7 shows the growth rate obtained as a function of substrate temperature in a mixture of silane in O_2 (7%) for films grown with the lamp off (conventional pyrolytic CVD) and (under identical conditions) during irradiation. Also shown are typical photo-CVD results recently obtained with silane/N_2O mixtures [11]. In the 100–350°C range, the fastest growth rates by far are achieved by photo-decomposition of the silane/oxygen mixture. In fact, at 300°C, the growth by photo deposition is nearly 500% faster than the equivalent thermal reaction, while at 200°C it is more than an order of magnitude more rapid than its thermal counterpart.

Optimised deposition conditions have produced, at ~~ ~, SiO_2 films with refractive indices of 1.46, etch rates of 20 Å/min in diluted 1 : 25 buffered HF : H_2O, and electrical breakdown fields of 5 to 8 MV/cm. These properties are very close to those obtained for thermally grown stoichiometric SiO_2 grown at temperatures around 800°C [38].

Fig. 8 shows the FTIR spectra obtained from films grown under different ratios of ammonia and nitrous oxide, whose reflective indices varied from 1.48 to 1.85. A clear transition from a Si–N (845 cm^{-1}) predominant vibration mode to a Si–O (1065 cm^{-1}) is strongly visible in the spectra, and this corresponds directly to the change in refractive index. A smooth progression from silicon nitride to silicon oxide can thus be achieved, and good control of the SiO_xN_y stoichiometry and hence the optical properties of the films grown is available with this deposition technique. This ability to selectively predetermine the composition of the reactive precursors which will ultimately react with the silane gives this photo-CVD process an added advantage over conventional plasma deposition.

4.3. Oxidation of silicon

More recent work on the direct photo-oxidation of silicon at low temperature (250°C) has shown the reaction rate is more than three times greater than that for UV-induced oxidation of silicon using a typical low pressure mercury lamp at 350°C. Fig. 9 shows the film thickness produced as a function exposure time for different oxidation techniques using an excimer lamp, ozone, low pressure mercury lamp, visible radiation and thermal oxidation. As can be seen, the oxidation rate using excimer lamp is much higher than that using ozone, Hg-lamp or visible irradiation. Thermal oxidation is negligible at 450°C even after long space reaction times of up to 5 h. Capacitance-voltage measurements at 10 kHz on MOS structures formed using Al gate contacts showed promising electrical proper-

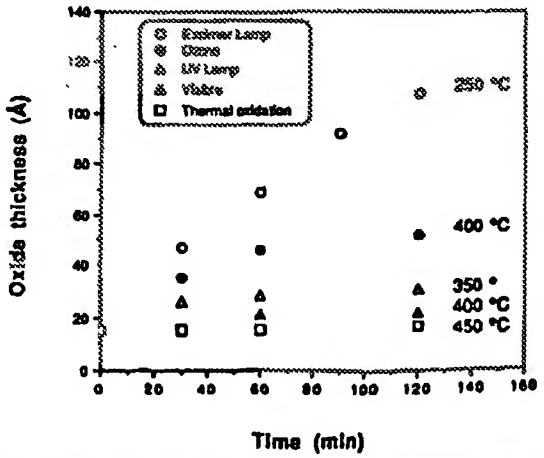

Fig. 9. Comparison of oxide thicknesses formed on Si for different light irradiation conditions and thermal oxidation with O_2 and O_3.

ties. More detailed results of this work will be published soon [39]. Thus excimer UV induced low temperature oxidation of Si also appears to be very attractive for future ULSI technology.

4.4. Other applications

The applications of excimer UV sources have also been demonstrated in several other areas recently, such as UV curing of paints, varnishes and adhesives [40,41], surface modification [33,42–44], and photo-degradation of a variety of pollutants [45–48].

The photo-degradation or photo-etching of different polymers is also possible using different wavelengths (172 nm, 222 nm and 308 nm) [33,42–44]. The considerably higher material removal rates obtained under these conditions suggest that excimer UV sources could also find applications in the microstructuring of large area polymer surfaces.

UV curing is the name given to the polymerisation of special paints, varnishes, adhesives and sealing or casting compounds as a result of their exposure to such radiation. UV curing of paints and transparent varnishes is already used for metal, wood, paper, plastic parts, foils compact discs and glass fibres. Polymer coatings are applied to metal mainly to provide protection against corrosion or for decorative purposes. Experimental results have shown that excimer VUV and UV sources are ideal for initiating the photo-polymerisation processes because of very rapid polymerization at ambient temperature [40,41].

The photochemical processing potential of these devices has been recognised and various groups are investigating their use in a variety of environmental and industrial situations. Kogelschatz et al. [45–48] have proposed designs for photoreactors incorporating excimer UV lamps as integral elements to undertake photodegradation of pollutants. These photo-induced processes will require high radiation intensities, probably at specific VUV/UV wavelengths, to be of practical or commercial interest.

Acknowledgement

The authors would like to thank Dr U. Kogelschatz (ABB, Switzerland) for many stimulating discussions. This work was supported by EPSRC (grant No. GR/J47750).

References

[1] D.J. Ehrlich, J.Y. Tsao, J. Vac. Sci. Technol. B 1 (1983) 969.
[2] I.W. Boyd, Laser Processing of Thin Films and Microstructures, Springer Series in Materials Science Vol. 3 (Springer, Berlin, 1987).
[3] F.W. Cross, R.K. Al-Dhahir, P.E. Dyer, A.J. MacRobert, Appl. Phys. Lett. 50 (1987) 1019.
[4] P.E. Dyer, in: Photochemical Processing of Electronic Materials, eds. I.W. Boyd, R.B. Jackman (Academic Press, London, 1992) p. 359.
[5] H. Esrom, G. Wahl, Chemtronics 4 (1989) 216.
[6] A. Auerbach, Appl. Phys. Lett. 47 (1985) 669.
[7] C.M. Harish, V. Kumar, A. Prabhakar, J. Electrochem. Soc. 135 (1988) 2903.
[8] B. Gellert, U. Kogelschatz, Appl. Phys. B 52 (1991) 14.
[9] B. Eliasson and U. Kogelschatz, Appl. Phys. B 46 (1988) 299.
[10] H. Esrom, J. Demny and U. Kogelschatz, Chemtronics 4 (1989) 202.
[11] P. Bergonzo, U. Kogelschatz, I.W. Boyd, Appl. Surf. Sci. 69 (1993) 393.
[12] G.A. Volkova, N.N. Kirillova, E.N. Pavlovskaya, A.V. Yakovleva, J. Appl. Spectrosc. 41 (1984) 1194.
[13] U. Kogelschatz, Pure Appl. Chem. 62 (1990) 1667.
[14] B. Eliasson, B. Gellert, J. Appl. Phys. 68 (1990) 2026.
[15] B. Eliasson, M. Hirth, U. Kogelschatz, J. Phys D 20 (1987) 1421.
[16] C. Duzy and J. Boness, IEEE J. Quant. Electron. QE-16 (1980) 640.
[17] O. Dutuit, R.A. Gutchek and J. Lecalve, Chem. Phys. Lett. 58 (1978) 66.
[18] N. Thonnard and G.S. Hurst, Phys. Rev. A 5 (1972) 1110.
[19] P. Moerman, R. Boucique and P. Mortier, Phys. Lett. 49 A (1974) 179.
[20] M. Kitamura, K. Mitsuka, and H. Sato, Appl. Surf. Sci. 79/80 (1994) 507.
[21] D.J. Eckstrom, H.H. Nakano, D.C. Lorents, T. Rothem, J.A. Betts, M.E. Lainhart, D.A. Dakin, J.E. Maenchen, J. Appl. Phys. 64 (1988) 1679.
[22] D.J. Eckstrom, H.H. Nakano, D.C. Lorents, T. Rothem, J.A. Betts, M.E. Lainhart, K.J. Triebès, D.A. Dakin, J. Appl. Phys. 64 (1988) 1691.
[23] U. Kogelschatz, Appl. Surf. Sci. 54 (1992) 410.
[24] B. Eliasson, U. Kogelschatz, IEEE Trans. Plasma Sci. 19 (1991) 309.
[25] Ch.K. Rhodes, Excimer Lasers (Springer, Berlin, 1984).
[26] A. Gilbert, J. Baggot, Essential of Molecular Photochemistry (Blackwell Scientific, Oxford, 1991).
[27] M.P. Golde and A. Kvaran, J. Chem. Phys. 72 (1980) 434.
[28] M.E. Gross, G.J. Fisanick, P.K. Gallagher, K.J. Schnoes, M.D. Fennell, Appl. Phys. Lett. 47 (1985) 923.
[29] G.J. Fisanick, M.E. Gross, J.B. Hopkins, M.D. Fennell, K.J. Schnoes, A. Katzir, J. Appl. Phys. 57 (1985) 1139.
[30] M.E. Gross, A. Appelbaum and P.K. Gallagher, J. Appl. Phys., 61 (1987) 1628.
[31] U. Kogelschatz, Appl. Surf. Sci. 54 (1992) 410.
[32] H. Esrom and U. Kogelschatz, Thin Solid Films 218 (1992) 231.
[33] J.-Y. Zhang, Thesis, Karlsruhe University, Germany (1993).
[34] J.-Y. Zhang, H. Esrom and I.W. Boyd, Appl. Surf. Sci. 96–98 (1996) 399.
[35] H. Esrom and U. Kogelschatz, Appl. Surf. Sci. 46 (1990) 158.
[36] P. Bergonzo, I.W. Boyd, J. Appl. Phys. 76 (1994) 4372.
[37] P. Bergonzo and I.W. Boyd, Appl. Phys. Lett. 63 (1993) 1757.
[38] T.T. Chan, S.R. Mejia, K.C. Kao, J. Electrochem. Soc. 138 (1991) 325.

[39] J.-Y. Zhang and I.W. Boyd, to be published.
[40] R.S. Nohr and J.G. MacDonald, Radiat. Phys. Chem. 46 (1995) 983.
[41] U. Kogelschatz, B. Eliasson and H. Esrom, Mater. Design 12 (1991) 251.
[42] H. Esrom, J.-Y. Zhang, and U. Kogelschatz, Mat. Res. Symp. Proc., Vol. 236 (MRS, Pittsburgh, 1992).
[43] J.-Y. Zhang, H. Esrom, U. Kogelschatz, G. Emig, Appl. Surf. Sci. 69 (1993) 299.
[44] J.-Y. Zhang, H. Esrom, U. Kogelschatz and G. Emig, J. Adhesion Sci. Technol. 8 (1994) 1179.
[45] H. Esrom, H. Scheyt, R. Mehnert and C. v. Sonntag, NATO Advanced Research Workshop on Non-thermal Plasma Techniques for Pollution Control, Cambridge UK, September 21–25 (1992).
[46] U. Kogelschatz, NATO Advanced Research Workshop on Non-thermal Plasma Techniques for Pollution Control, Cambridge, UK, September 21–25 (1992).
[47] R.S. Nohr and J.G. MacDonald, U. Kogelschatz, G. Mark, H.-P. Schuchmann and C. von Sonntag, J. Photochem. Photobiol. Chem. A 79 (1994) 141.
[48] M. Niwano, M. Suemitsu, Y. Ishibashi, Y. Takeda, N. Miyamoto, K. Honma, J. Vac. Sci. Technol. A10 (1992) 3171.